Available online at www.sciencedirect.com
ScienceDirect
Trans. Nonferrous Met. Soc. China 35(2025) 2747−2761
Transactions of Nonferrous Metals Society of China
www.tnmsc.cn

Diffusion characteristics of deep-sea mining sediment plumes in flowing water by large-scale water tank experiments

Ze-lin LIU[1], Xiang WU[1], Qiu-hua RAO[1], Wei YI[1], Shi-ping CHEN[2], Hao ZHENG[2]

1. School of Civil Engineering, Central South University, Changsha 410075, China;
2. State Key Laboratory of Exploitation and Utilization of Deep-sea Mineral Resources, Changsha Research Institute Mining and Metallurgy Co., Ltd., Changsha 410012, China

Received 10 November 2024; accepted 20 March 2025

Abstract: The existing deep-sea sediment plume tests are mostly under small-scale static water and rarely under large-scale flowing water conditions. In this study, large-scale tank experiments of flowing water were designed and conducted to investigate the morphological characteristics and concentration evolution of the sediment plumes under different discharge rates (Q) and initial sediment concentrations (c). Viscosity tests, resuspension tests and free settling tests of the sediment solution with different c values were performed to reveal the settling mechanism of the plume diffusion process. The results show that the plume diffusion morphology variation in flowing water has four stages and the plume concentration evolution has three stages. The larger the Q, the smaller the initial incidence angle at the discharge outlet, the larger the diffusion range, the poorer the stability and the more complicated the diffusion morphology. The larger the c, the larger the settling velocity, the faster the formation of high-concentration accumulation zone, the better the stability and the clearer the diffusion boundary. The research results could provide experimental data for assessing the impact of deep-sea mining on the ocean environment.

Key words: deep-sea mining; sediment plumes; diffusion characteristics; flowing water; large-scale water tank experiment

1 Introduction

With the increasing depletion of land mineral resources and the growing demand for mineral resources, human beings turned their attention to the deep sea, where there are abundant polymetallic nodules, cobalt-rich crusts and polymetallic sulfides [1−5], and thus the deep-sea mining has important economic and strategic significances. However, the mining vehicle operation would create sediment plumes with a large number of sediment particles and harmful substances (i.e., Cu, Cd, Zn, and Pb), and could spread over thousands of kilometers within a few decades [6], leading to an increment of suspended particles, turbidity (about 300%) and heavy metals (about 10 times), and a decrement of biological abundance (30%−50%) [7]. Therefore, in-depth research on the diffusion characteristics of deep-sea mining sediment plumes is of great significance for evaluating the environmental impacts of deep-sea mining [8−11].

At present, the diffusion characteristics of deep-sea mining sediment plumes have been studied theoretically, numerically and experimentally. In theoretical analyses, various models were proposed or adopted to study the behaviors of plume diffusion, e.g., Stokes' settling theory [12], Ouillon's convection−diffusion−settling model [13] and our new settling resistance coefficient model of irregular particles [3]. In numerical studies, there are numerous methods for simulating the plume

Corresponding author: Qiu-hua RAO, E-mail: raoqh@csu.edu.cn
https://doi.org/10.1016/S1003-6326(25)66845-2

evolution process, including CFD-DPM [14,15], Jankowski's model [16], MIT-gcm model [17], axisymmetric model [18], SPH (smooth particle hydrodynamics) method [19] and Euler two-fluid model [20]. The above theoretical models and numerical methods need to be verified by in-situ or laboratory tests of the plume diffusion.

In deep-sea in-situ tests, the plume diffusion characteristics were monitored by using acoustic, optical, and other methods. For example, researchers in Refs. [21−25] adopted an optical backscatter sensor (OBS), an acoustic doppler current profiler (ADCP) and an autonomous underwater vehicle (AUV) to measure the concentration and diffusion range of the sediment plume at the tropical seamount located 483 km southwest of the Canary Islands. MUNOZ-ROYO et al [22] used a pre-prototype tubercle collection vehicle (equipped with optical turbidity meters, internal pressure sensors and sediment concentration sensors) at a depth of 4500 m in the Clarion−Clipperton Zone to detect that 2%−8% of the sediment mass (at 2 m or higher above the seabed) did not settle within a few hours and that the other 92%−98% (below 2 m) settled locally and partially. Obviously, the complex deep-sea environment and limitations of testing technology pose significant challenges to the in-situ monitoring of plume diffusion. Consequently, laboratory experiments are commonly used. For example, BAINES [26] used a small cuboid water tank (60 cm × 30 cm × 30 cm in size) to record the plume diffusion in the layered fresh and saltwater by a camera, where the enrolling at the end of the plume would dilute the pollutants and the enrolling extent depended on the relative magnitude of the lateral and terminal enrolling flux. MOTT and WOODS [27] conducted a density stratified plume discharge test (double-layer) in a water tank (40 cm × 40 cm × 50 cm in size) and found that when the plume passed through the lower stratified fluid to reach the density interface, it might transform to be a fountain if the fluid density above the interface was smaller than the overall density of the plume. To sum up, the current lab tests of plume diffusion are mostly conducted in still water but less in flowing water. Considering the ocean current environment, it is essential to further explore the diffusion characteristics of deep-sea mining sediment plumes in flowing water.

In this study, large-scale water tank experiments were designed and conducted to investigate the morphological characteristics and concentration evolution of the deep-sea mining sediment plume under different discharge rates (Q) and initial sediment concentration (c) in flowing water firstly. Then, the viscosity test of the sediment solutions with different concentrations was employed to analyze the influence of the sediment solution concentration on the settling velocity. Finally, the resuspension settling test and the free settling test of sediment solutions with different concentrations were performed to reveal the mechanism of plume settlement in different stages of the plume diffusion.

2 Laboratory tests of sediment plume diffusion in flowing water

2.1 Water tank and test equipment

Figure 1 shows a cuboid water tank with 20 m × 1.5 m × 2.5 m in size, located in the State Key Laboratory of Exploration and Utilization of Deep Sea Mineral Resources of Changsha Research Institute of Mining and Metallurgy Co., Ltd., China. Its top is open for conveniently installing the instruments in different positions, the bottom is made of steel for bearing capacity, and the four sides are made of transparent glass for clear observation of the plume diffusion process.

The water tank is equipped with three systems: water circulation system, sediment discharge system and monitoring system. The water circulation system includes a water pump (for pumping the water at a constant flow rate), a water pipe (for transporting the water) and the rectifier panel (for ensuring a stable water-flow rate (v)). The sediment discharge system includes a storage container (for containing the sediment solution with an initial concentration c), a discharge outlet (coordinates x=8 m, y=0.75 m, and z=0.5 m, for discharging the sediment solution), a sediment discharge pump (for pumping the sediment solution at a constant discharge rate Q) and a flowmeter (for controlling and measuring the discharge rate Q of the sediment solution). The monitoring system includes an ADCP (for measuring the fluid velocity), 7 sets of Sinomeasure turbidimeters (for measuring the concentration distribution of the

plumes, which are equipped with an MLSS−530 sludge concentration sensor, measuring range of 0−4000 NTU, resolution of 0.2 NTU, accuracy of ±5% full scale, and calibrated by standard turbidity solution), and two cameras (for monitoring the top and side diffusion characteristics of the plumes). The coordinates of the ADCP and turbidimeter locations are shown in Fig. 2 and Table 1.

2.2 Test procedures

The water tank tests for the sediment plume diffusion in flowing water were conducted under

Fig. 1 Water tank and testing instruments for plume diffusion in flowing water: (a) Water tank; (b) Water pump; (c) Rectifier panel; (d) Discharge outlet; (e) Storage container; (f) Sediment discharge pump; (g) Flowmeter; (h) ADCP; (i) Sinomeasure turbidimeter; (j) Camera

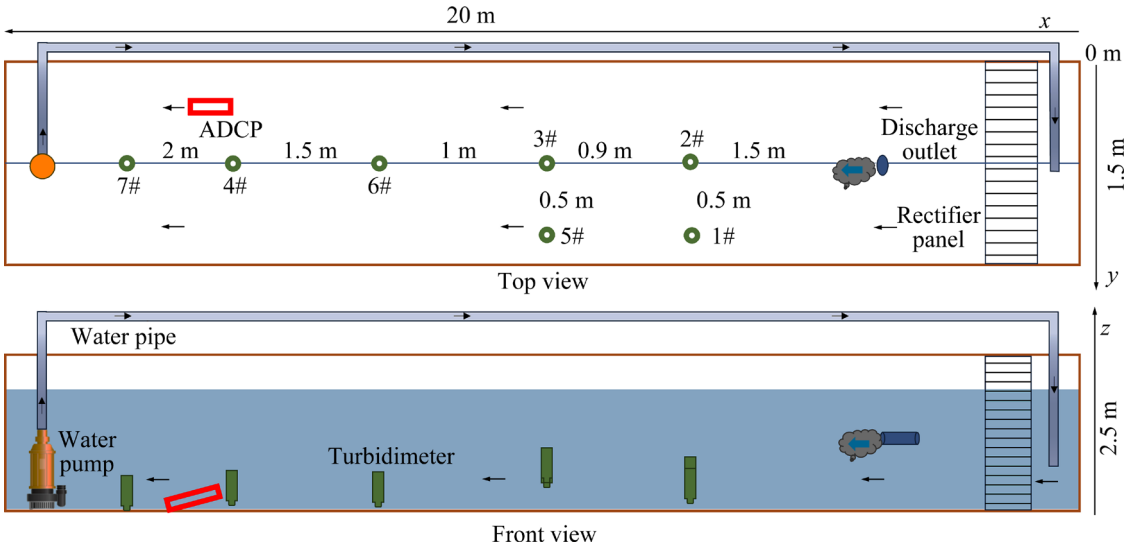

Fig. 2 Schematic diagrams of ADCP and turbidimeter location

Table 1 Coordinates of ADCP and turbidimeter location

Position	ADCP	Turbidimeter						
		7#	4#	6#	5#	3#	1#	2#
x/m	12.62	14.9	12.9	11.4	10.4	10.4	9.5	9.5
y/m	0.40	0.75	0.75	0.75	1.25	0.50	1.25	0.75
z/m	0.20	0.15	0.20	0.20	0.40	0.35	0.35	0.20

constant water-flow rates v, different initial concentrations c and discharge rates Q of sediment solution, as listed in Table 2, where Q and c were determined based on the requirements for the collection of 3×10^6 t of deep-sea polymetallic dry nodules per year. If 5−10 collecting vehicles were used to work simultaneously for 320 d per year and the collecting efficiency was 70%, the sediment discharge rate Q and initial concentration c could be calculated as c≈11.7−23.4 g/L and Q≈15−30 L/min.

Table 2 Test parameters in flowing water by large-scale water tank

Group	v/(cm·s^{-1})	c/(g·L^{-1})	Q/(L·min^{-1})
a	1	10	15
b	1	10	30
c	1	20	15
d	1	20	30
e	1	30	15
f	1	30	30

The test procedures were illustrated as follows.

(1) Prepare the sediment solution. Deep-sea sediments (d_{50}=7.43 μm, Fig. 3) were collected from the Pacific mining area at a depth of 5200 m. According to its water content, the sediment solutions with the same volume (V=40 L) but different concentrations were prepared, by using a stirrer (equipped with a stirring rod of 12 cm in diameter and at a speed of 1000 r/min) to fully disperse and stir the sediment mixed with tap water (about 3 min) until there were no large lumps in the solution.

(2) Start the circulation of flowing water. The tap water in the water tank was extracted by one water pump at the left end and then transported to the right end by a long soft pipe to realize the water circulation (i.e., flowing water). The water-flow rate v was monitored by an ADCP (Fig. 2) and kept to be constant (Table 2).

(3) Start and stop the discharge of the sediment solution. The sediment solution of 40 L in volume was pumped into the water tank by another water pump until it was pumped out completely. During this process, the real-time discharge rate Q, the plume diffusion concentration and morphological characteristics were monitored by a flowmeter (Fig. 1(g)), a turbidimeter (Fig. 1(i)) and a camera (Fig. 1(j)), respectively.

(4) Stop the water circulation. When the sediment plume was diffused to the vicinity of the water pump at the left end, turn off the water pump to stop the water circulation (i.e., still water). And then, the sediment plume diffusion in the water tank was mainly characterized by settlement. The test was stopped until the plume concentration (monitored by the turbidimeter) was almost unchanged (for 1−3 h).

(5) Data processing and analysis. The collected data were processed and analyzed, including morphological characteristics and concentration of the plume diffusion.

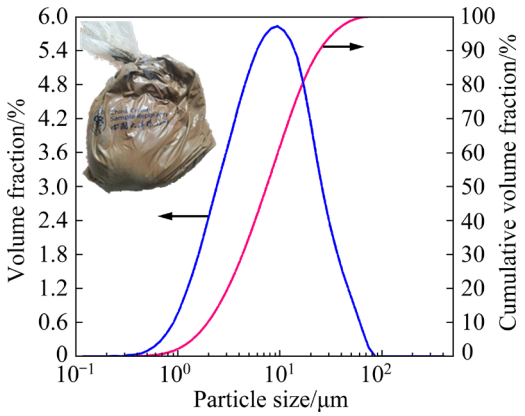

Fig. 3 Distribution of sediment particle size

2.3 Test results and analyses

2.3.1 Morphological characteristics of plume diffusion near discharge outlet

Figure 4 shows morphological characteristics of the plume diffusion in the flowing water (at constant water-flow rate) near the discharge outlet (within 2.5 m) under different initial concentrations of the sediment solution c and different discharge rates Q of the sediment solution, where the time of last figure in each group corresponds to the discharge completion. It is seen that the plume diffusion can be divided into four stages: (1) Jet-spreading stage (where the sediment solution is ejected from the discharge outlet to form the plume along x-direction); (2) Settlement−rebounding−resettlement stage (where the sediment plume mainly settles down to the bottom and then rebounds in three-dimensional direction to form a high concentration region); (3) Diffusion-transportation stage (where the sediment plume was diffused with decreasing concentration and transported with the flowing water); (4) Dilution−resettlement stage (when its concentration is gradually diffused

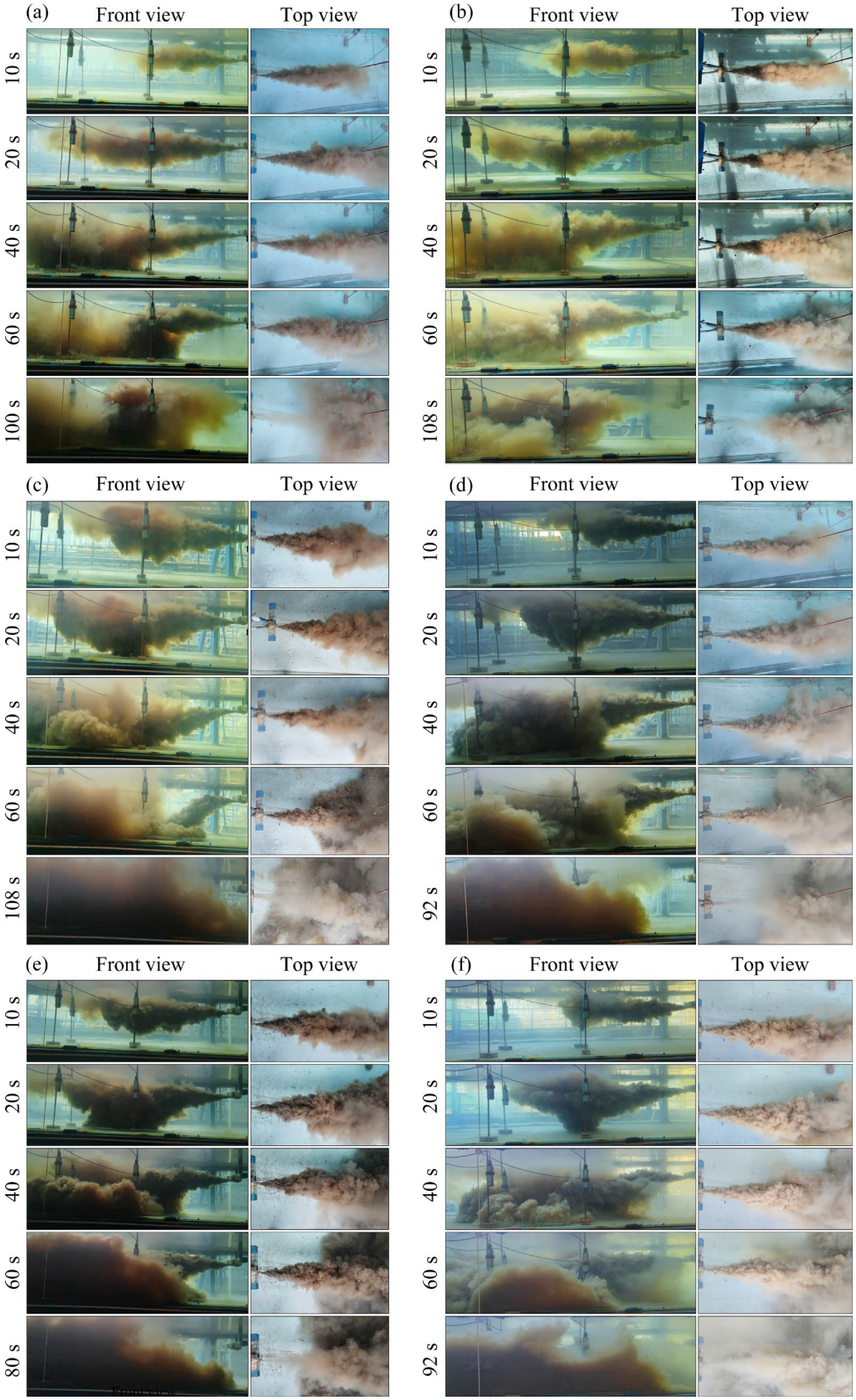

Fig. 4 Morphological characteristics of plume diffusion process in flowing water tank near discharge outlet under different initial concentrations of sediment solutions and discharge rates: (a) c=10 g/L, Q=15 L/min; (b) c=10 g/L, Q=30 L/min; (c) c=20 g/L, Q=15 L/min; (d) c=20 g/L, Q=30 L/min; (e) c=30 g/L, Q=15 L/min; (f) c=30 g/L, Q=30 L/min

to be the same as that of the surrounding water, the plume diffusion would stop in space and there is only free settlement in z-direction).

Under the same initial solution concentration c and different discharge rates Q (e.g., Figs. 4(a) and (b); Figs. 4(c) and (d); Figs. 4(e) and (f)), the three groups of plume diffusion process would appear similar morphological characteristics. As the discharge rate Q is increased from 15 to 30 L/min, the plume has a smaller initial incident angle at the discharge outlet (e.g., from 30° and 26.7° under c=10 g/L), a larger increase of diffusion range at the same time (e.g., Figs. 4(a) and (b)), poorer stability and more complicated diffusion morphology (e.g., more obvious entrainment effect in the x-direction, see the last figure in each group). That is because a larger Q (greater sediment mass and velocity) can provide a greater initial momentum for the plume to be injected out rapidly along the discharge direction at a smaller initial incident angle. At the same time, a greater momentum enables the plume to overcome the resistance and interference of the surrounding water body and to spread into a larger diffuse range. Besides, when Q is increased, v is also increased to prompt the turbulence generation (according to the Reynolds number Re, $Re=\rho_f vd/\mu$, where ρ_f, v, d and μ are fluid density, flow rate, characteristic length and dynamic viscosity, respectively) and the larger velocity gradient leads to the increased shear. Thus, the interaction between the plume and the surrounding water is stronger and the formation of reflux and vortex is easier, resulting in more unstable and more complicated diffusion morphology.

Under the same discharge rate Q and different initial solution concentrations c (e.g., Figs. 4(a), (c), and (e); Figs. 4(b), (d), and (f)), the two groups of plume diffusion processes appear similar morphological characteristics. As the solution concentration c is increased from 10 to 30 g/L, the plume has a larger settling velocity in the vertical direction (e.g., the time of the plume settling to the bottom is 20 s in Fig. 4(e) and 40 s in Fig. 4(a)), faster formation of high-concentration accumulation zone near the discharge outlet (e.g., the formation time is 20 s in Fig. 4(e) and 10 s in Fig. 4(a)), and a larger high-concentration accumulation zone during the plume diffusion. That is because the higher the concentration of the initial sediment solution, the larger the gravity ($F=(\rho_p-\rho_f)gV$, where F, ρ_p, g and V are difference between gravity and buoyancy, particle density, gravitational acceleration and volume, respectively), and therefore the larger the settling velocity. Furthermore, the sediment solution of a higher concentration has a larger viscosity, which hinders the movement of particles and creates a smaller diffusion rate and less turbulent flow of the plume with a more obvious concentration gradient at the diffusion boundary. As a result, it is faster to form a larger high-concentration accumulation zone.

In addition, Fig. 5 illustrates morphological characteristics of the plume diffusion leading-end in the flowing water tank under different initial sediment solution concentrations c and different discharge rates Q. It is seen that under the same c (Figs. 5(a) and (b); Figs. 5(c) and (d); Figs. 5(e) and (f)), the three groups of plume diffusion leading-end appear similar morphological characteristics. As the discharge rate Q is increased from 15 L/min (e.g., Fig. 5(e)) to 30 L/min (e.g., Fig. 5(f)), the plume diffusion leading-end shape is gradually changed from a relatively smooth-regular curve boundary to a rough-irregular “mushroom clouds” boundary (i.e., accompanied by a large number of folds, protrusions and depressions). That is because under the same initial concentrations, a higher discharge rate would provide a greater momentum for the plume to mix intensely with the surrounding water body, resulting in a more complex leading-end shape controlled by turbulence and eddies.

Under the same discharge rate Q (Figs. 5(a), (c), and (e); Figs. 5(b), (d), and (f)), the two groups of plume diffusion leading-end also have similar morphological characteristics. When the initial solution concentration c is increased from 10 g/L (e.g., Fig. 5(a)) to 30 g/L (e.g., Fig. 5(e)), the plume diffusion leading-end shape is gradually changed from a relatively smooth-regular curve boundary to a rough-irregular “mushroom clouds” boundary, since the lower the concentration, the weaker the interaction between the particles, and thus the easier the plume free diffusion.

2.3.2 Evolution of plume diffusion concentration

Figure 6 shows tested curves of the plume diffusion concentration varying with time at different positions (1#−7# in Fig. 2). They are all divided into three stages: rapid rising stage, rapid

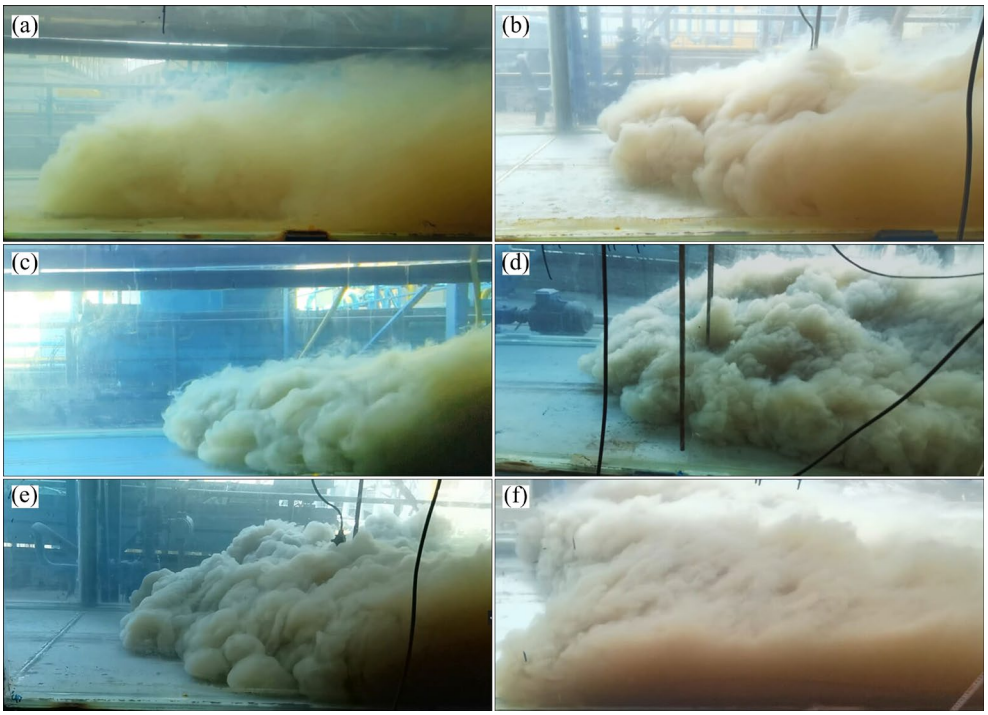

Fig. 5 Morphological characteristics of plume diffusion leading-end in flowing water tank under different initial concentrations of sediment solutions and discharge rates: (a) c=10 g/L, Q=15 L/min; (b) c=10 g/L, Q=30 L/min; (c) c=20 g/L, Q=15 L/min; (d) c=20 g/L, Q=30 L/min; (e) c=30 g/L, Q=15 L/min; (f) c=30 g/L, Q=30 L/min

dropping stage, and slow dropping to be almost unchanged. In order to analyze the changing process more clearly, take the monitoring curve of sensor 4# (Fig. 6(h)) as an example. Firstly, the plume concentration is linearly increased from 0 to the peak concentration (413 mg/L), due to the continuous release of plume particles from the discharge outlet. As the plume particles are gradually accumulated and moved with the water flow, their mixing with the surrounding water reaches a relatively stable state and therefore the concentration no longer continues to increase. Then, the plume concentration dropped fast because the plume is continuously diffused and gradually diluted by the surrounding water, where the large sediment particles rapidly settle down. Finally, the plume concentration is decreased slowly to approach a relatively stable value, because mixing the plume and the surrounding water gradually reaches a dynamic equilibrium as time passes. During the continuous diffusion of the plume, the large particles mostly settle down to the water tank bottom, and the fine particles are mainly moved and gradually diluted by the surrounding water, resulting in a slight decrease of the plume concentration until final stability. Also, it is found that under the same height in the discharge direction (e.g., 0.2 m), the plume concentration shows a gradually decreasing trend as time goes on (Fig. 6(g)), i.e., the plume is gradually diffused from the high-concentration areas to the low-concentration areas. That is caused by the gradual settling of the solid particles in the plume due to gravity and the dilution effect of the surrounding water.

Obviously, the plume diffusion concentration is greatly influenced by the discharge rate Q and initial solution concentration c. Under the same c, the larger the Q, the greater the driving force for greater sediment transportation at the same time and therefore the faster the increase of in plume concentration during the first stage. And then in the second stage, the larger the Q, the more quickly and fully the mixing of the plume with the surrounding water (i.e., the greater dilution effect), and therefore the faster the decrease in plume concentration to a lower stable value in the third stage (e.g., the stable plume concentrations at Q=15 and 30 g/L are 17.4 and 14.7 mg/L, respectively, in Figs. 6(e) and (f) at the 6# turbidimeter).

In addition, under the same Q, the larger the c, the more the number of particles per unit volume in

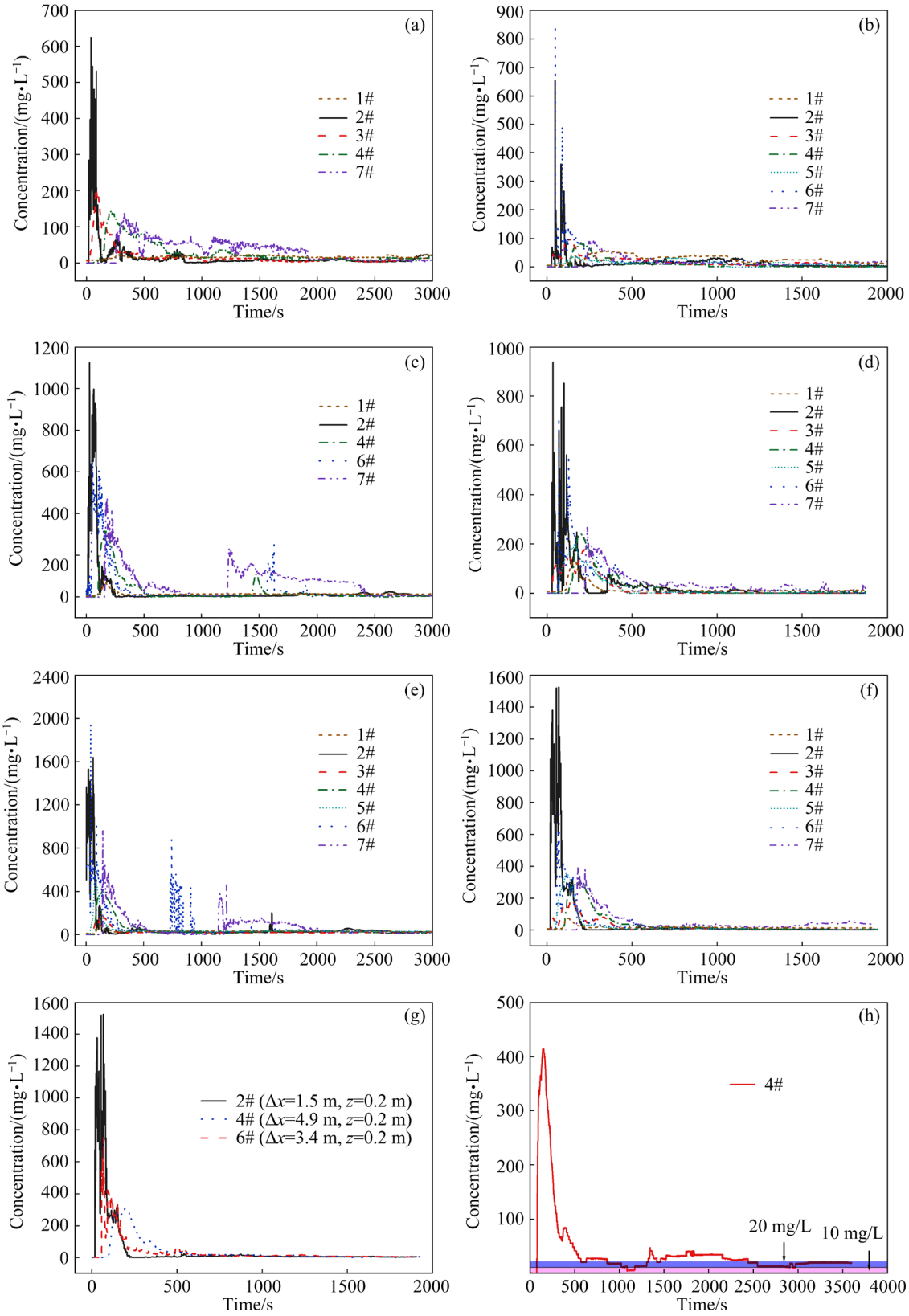

Fig. 6 Tested curves of plume diffusion concentration varying with time at different positions under different discharge rates and initial concentrations of sediment solutions: (a) Q=15 L/min, c=10 g/L; (b) Q=30 L/min, c=10 g/L; (c) Q=15 L/min, c=20 g/L; (d) Q=30 L/min, c=20 g/L; (e) Q=15 L/min, c=30 g/L; (f) Q=30 L/min, c=30 g/L; (g) Concentration curves at same height (Q=30 L/min and c=30 g/L); (h) Concentration curve of 4# turbidimeter (Q=15 L/min and c=30 g/L)

the sediment solution, the faster the diffusion of more particles to the monitoring point and therefore the faster the increase in plume concentration and the higher the peak value in the first stage (e.g., the peak plume concentrations with c=10 and 30 g/L are 625 and 1640 mg/L, respectively, in Figs. 6(a) and (e) at the 7# turbidimeter). In the second stage, the larger the c, the stronger the interactions between particles and the faster the diffusing and settling processes, resulting in a faster decrease of the plume concentration. In the third stage, the sediment plume with a larger c has more particles and more difficulty in dilution and therefore higher final concentration (e.g., the stable plume concentrations with c=10 and 30 g/L are 14.4 and 18.5 mg/L, respectively, in Figs. 6(a) and (e) at the 7# turbidimeter).

3 Laboratory tests of sediment plume settlement in still saltwater

In the above large-scale water tank experiments, the sediment plume diffusion in flowing water has four stages of jet-spreading (Stage 1), settlement−rebounding−resettlement (Stage 2), diffusion−transportation (Stage 3) and dilution−resettlement (Stage 4). Since there is difficulty in measuring the settlement-velocity of the sediment plume in the long water tank, the resuspension test and free sedimentation tests of the sediment solutions in still salt water (instead of ordinary water for simulating the actual sea water) were carried out to further investigate the plume diffusion mechanism in Stage 2 and Stage 4 (both are involved to the settlement). Considering that the initial concentration of the sediment solution (related to its viscosity) is a main factor influencing the plume settling velocity, it is necessary to conduct the viscosity test of the sediment solutions with different concentrations before the resuspension and free sedimentation tests.

3.1 Viscosity test of sediment solutions with different concentrations

3.1.1 Test arrangement

Figure 7 shows the viscosity test procedure of the sediment solutions with different concentrations, which were prepared by the following steps: (1) mix the artificial seawater salt (165 g, according to the salt/water mass ratio of 33:100) with water completely to prepare the seawater solution of 5 L; (2) measure the water content of deep-sea sediments (w) by $w=(m_1-m_2)/m_2\times100\%$ (where m_1 is wet mass, and m_2 is dry mass after the sediments are placed in an oven at 105 °C for 12 h and then cooled to room temperature); (3) put the deep-sea sediments of m_1 into a breaker, and then add a certain amount of seawater into the breaker (containing the sediments) to reach the required volume (V) in order to prepare the sediment solutions with different concentrations c (10, 20, 30, 40, and 50 g/L) by $c=m_2/V= Vm_1/(1+w)$.

The NDJ−1S digital viscometer (with a speed of 60 r/min, a maximum measuring range of 10 mPa·s and an accuracy of 0.01 mPa·s) was used to measure the viscosity of deep-sea sediment solutions with different c. The tests were repeated 3 times after the sediment solution was gently stirred to blend evenly and the average value was regarded as the viscosity of deep-sea sediment solutions.

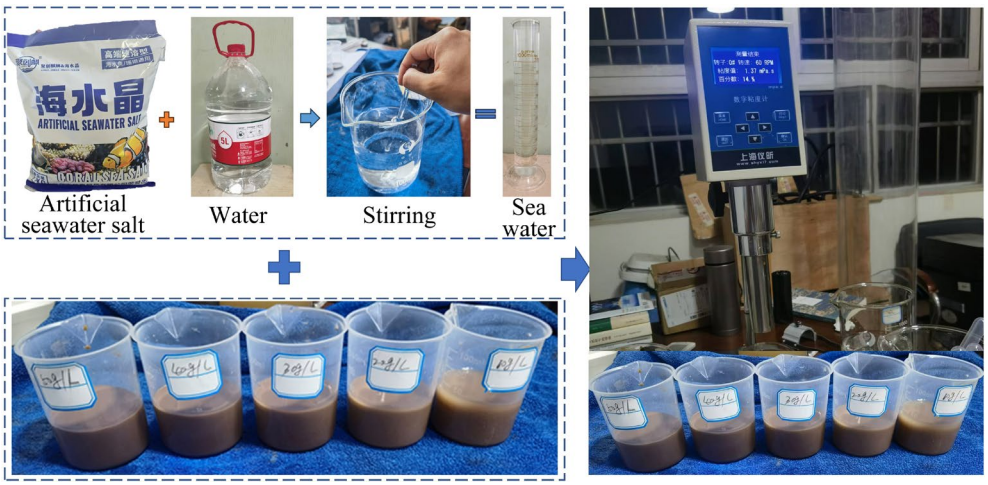

Fig. 7 Viscosity test process of sediment solutions with different concentrations

3.1.2 Test results and analyses

Table 3 and Fig. 8 show the tested viscosity results of the deep-sea sediment solutions with different initial concentrations (three times for each concentration). Obviously, the viscosity of the sediment solution (η) gradually increases with the increase in the concentration c (e.g., the viscosity of the 50 g/L sediment solution is 2.59 times that of the 10 g/L sediment solution). The higher the concentration of sediment solution, the greater the number of particles per unit volume (i.e., the smaller the spacing between particles), resulting in the larger interaction forces and thus the poor fluidity and the more viscous solution. The relationship between the c and η can be expressed by the fitting curve with the test results:

$$\eta=0.5637\exp(c/29.2908)+0.59,\quad R^2=0.99 \tag{1}$$

Table 3 Tested viscosity results of sediment solutions with different initial concentrations

c/(g·L^{-1})	η/(mPa·s)			Mean value of η/(mPa·s)
	First time	Second time	Third time	
0	1.12	1.15	1.10	1.12
10	1.37	1.46	1.46	1.43
20	1.78	1.78	1.75	1.77
30	2.09	2.02	2.07	2.06
40	2.88	2.86	2.81	2.85
50	3.69	3.71	3.69	3.70

Considering that the initial concentration of sediment solution (related to its viscosity) is a main factor influencing the plume settling velocity, it is necessary to conduct the viscosity test of the sediment solutions with different concentrations before the resuspension and free sediment tests. It is well known that the initial concentration of sediment solution (directly proportional to its viscosity in Eq. (1)) has a great influence on the plume settling velocity. According to the Stokes' law, the settling velocity of particles in a liquid is inversely proportional to the liquid viscosity. The sediment solution with high viscosity would produce a greater resistance to the settling process and a smaller settling velocity. In addition, the higher the viscosity of the sediment solution, the smaller the particle perturbation and the more difficult the violent movements and collisions. Therefore, it is more helpful to maintain the suspended state of the sediment particles.

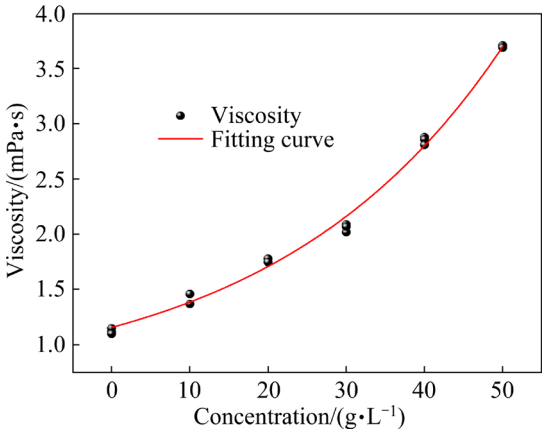

Fig. 8 Tested viscosity results and fitting curve of sediment solutions with different initial concentrations

3.2 Resuspension test of sediment solutions with different concentrations

3.2.1 Test arrangement

Figure 9 shows the resuspension test apparatus for the sediment solutions. Similarly to Section 3.1, the sediment solutions (1 L in volume) with different initial concentrations c (c=10, 20 and 30 g/L) were prepared by the seawater and put in a settling cylinder (d62 mm × h420 mm). When they were stirred gently, mixed fully and then settled freely (i.e., resuspension test), a plastic tape (stuck at the left boundary of the settling cylinder) was used to measure the settling height h (for calculating the settling velocity), and a camera was used to record the settling process, where a backcloth and a backlight were adopted to improve the contrast and brightness of photos.

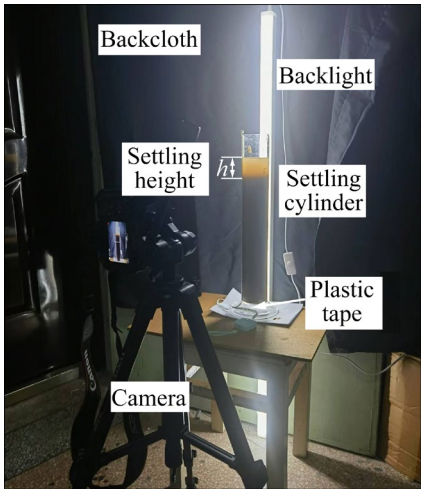

Fig. 9 Resuspension test apparatus for sediment solutions

3.2.2 Test results and analyses

Figure 10 shows camera photos for the resuspension process of the sediment solutions with different initial concentrations. They appear the similar characteristics: when the sediment solutions were stirred gently, mixed fully and then settled freely, the interface between the sediment solutions (in dark color) and the saltwater (in light color) is gradually moved down and becomes increasingly obvious as the time goes on, since the sediment settled by its gravity to gradually form a density stratification of the solution in the settling cylinder. Differently, at the same time, the low-concentration solution (e.g., 10 g/L in Fig. 10(a)) had a smaller density and thus a larger settling height h than the high-concentration solution (e.g., 20 g/L in Fig. 10(b)).

Figure 11 shows the settling velocity (w_t) varying with time for the sediment solutions with different initial concentrations. The curves in Fig. 11 were all divided into three stages: (1) fast increasing stage (the large particles in the sediment solution settled rapidly towards the cylinder bottom due to gravitational acceleration); (2) fast decreasing stage (the fine particles changed their settling direction under the fluid resistance and diffusion action, which reduced their settling velocity in the vertical direction); (3) slowly decreasing stage until stability (the settling velocity remains stable when the gravity of fine particles is balanced with the resistance, e.g., generated by the particle interaction, the Brownian motion and the weak convection of the fluid).

Besides, the settling velocity w_t is greatly affected by the sediment solution concentration c. In the first stage, the higher the c, the smaller both the growth rate and the peak value of w_t (except c=20 g/L, probably due to experimental errors). Since the particles in the higher-concentration solution with smaller spacing are more easily disturbed by the surrounding particles, they need to overcome larger fluid resistance to settle. Therefore, the growth rate and the peak value of w_t are smaller. And then, in the second stage, the

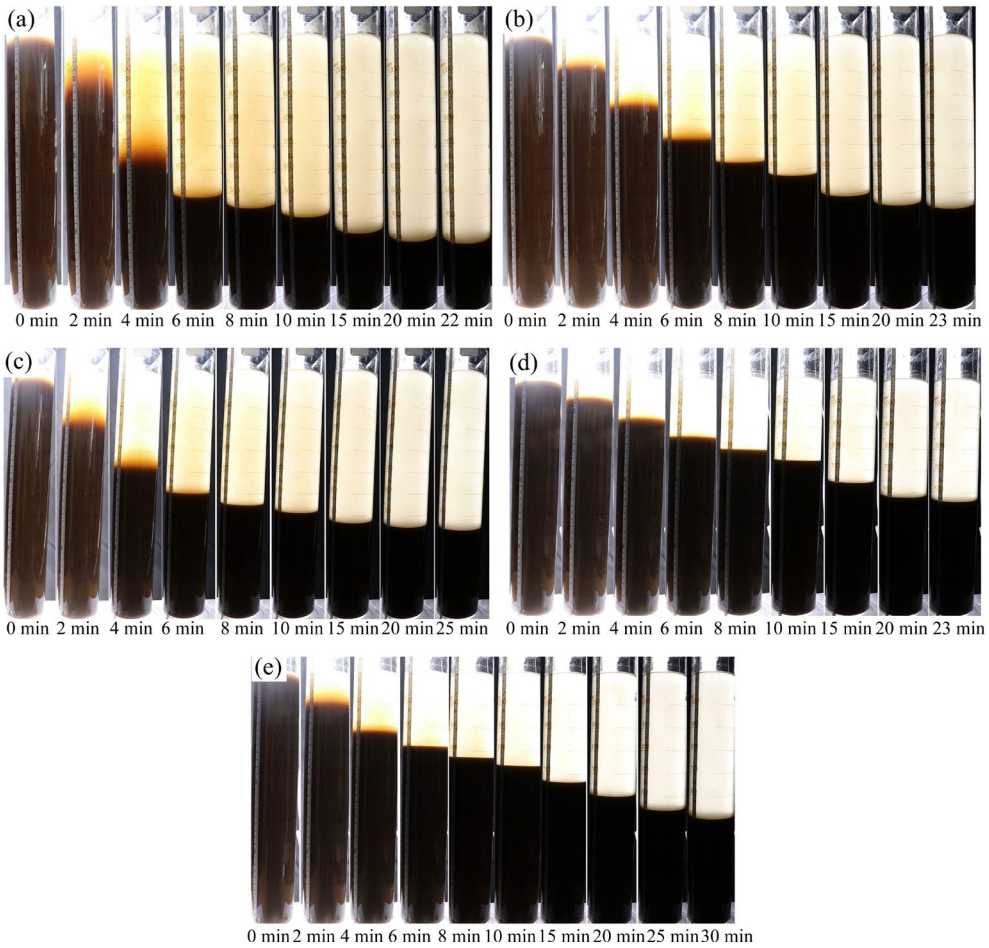

Fig. 10 Camera photos for resuspension processes of sediment solutions with different initial concentrations: (a) c=10 g/L; (b) c=20 g/L; (c) c=30 g/L; (d) c=40 g/L; (e) c=50 g/L

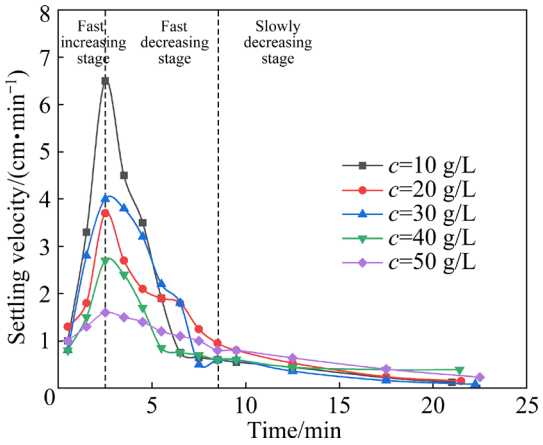

Fig. 11 Resuspension settling velocity varying with time for sediment solutions with different initial concentrations

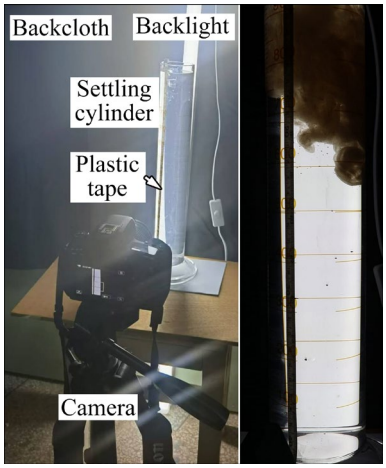

Fig. 12 Free settlement test apparatus of sediment solutions in still seawater

higher the *c,* the smaller the drop rate of w_t (except c=20 g/L), since the particles in the higher-concentration solution are subjected to higher fluid resistance and inter-particle interactions (e.g., collisions) during the settling process. Finally, in the third stage, the sediment solutions with higher concentrations have a slightly larger stable value of w_t (except c=20 g/L), since the particles with higher-concentration solution would form a more stable sediment structure for reducing the tumbling of the particles and the effect of fluid resistance on the settling velocity, and would make the settling process less disturbed for improving w_t.

3.3 Free settlement test of sediment solutions with different concentrations

3.3.1 Test arrangement

Figure 12 shows the free settlement test apparatus for the sediment solutions with different initial concentrations in still seawater, where the sediment solutions (5 mL with c=10, 20, 30, 40 and 50g/L) and testing system are the same as those in the resuspension test (Section 3.2). Differently, a pipette (diameter d=1 cm) is needed to release the well-mixed sediment solution into the settling cylinder slowly and uniformly.

3.3.2 Test results and analyses

Figure 13 shows the camera photos for the free settlement process of the sediment solutions with different initial concentrations. They also appeared the similar characteristics. Firstly, the coarse particles in the sediment solution settled rapidly due to larger momentum and smaller resistance at the initial time. And then the fine particles were diluted by the surrounding seawater and finally the sediment solutions were completely dissolved to be uniform solutions. Differently, at the same time, the higher the concentration (e.g., 10 g/L in Fig. 13(a) and 30 g/L in Fig. 13(c)), the larger the "particle clumps" and drag force (generated by disturbing the surrounding water) and thus the larger the settlement distance and particle amount.

Figure 14 shows the free settling velocity w_t varying with time for the sediment solutions with different concentrations. The curves in Fig. 14 were all divided into two stages: (1) rapidly decreasing stage, i.e, the coarse particles with greater mass were first to settle down at a large w_t and then the w_t slows down fast, since the settlement of the former particles would cause a wave behind them to form a vortex for greatly increasing the resistance of the subsequent particle settlement; (2) slowly decreasing to be stable stage, i.e., when the gravity, buoyancy and resistance of the particles gradually reached equilibrium, the settling process of the particles tends to be stable with almost unchanged w_t.

Similarly to the resuspension test, the free settling velocity w_t is also influenced by the sediment solution concentration c. In the first stage of rapidly decreasing, the high-concentration solution (e.g., 50 g/L) has a larger reduction rate of w_t than the low-concentration solutions (e.g., 10 g/L), since the larger the c, the larger the gravity

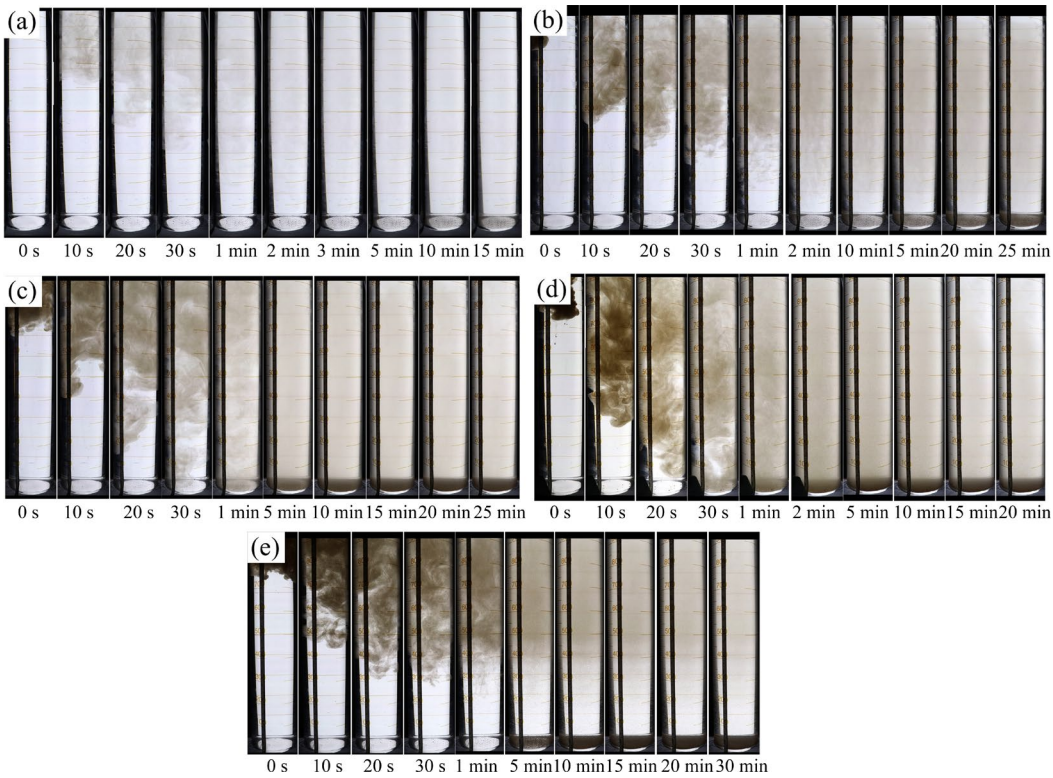

Fig. 13 Camera photos showing free settlement processes of sediment solutions with different initial concentrations: (a) c=10 g/L; (b) c=20 g/L; (c) c=30 g/L; (d) c=40 g/L; (e) c=50 g/L

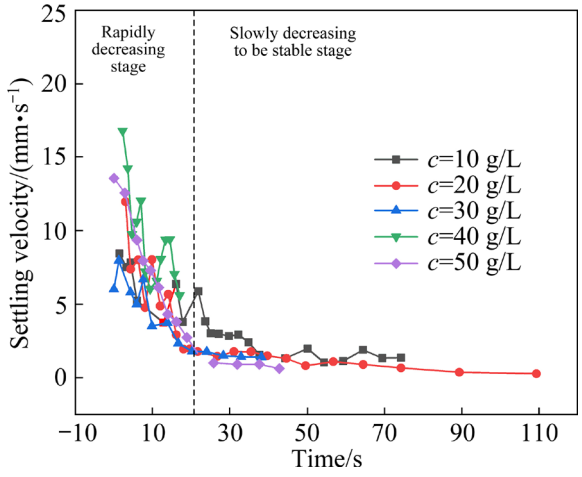

Fig. 14 Free settling velocity varying with time for sediment solutions with different initial concentrations

and the viscosity, the more frequently the particle collision, and thus the faster the resistance increase. In the second stage, the final settling velocity of the high-concentration solution is almost close to that of the low-concentration solution, since the sediment solutions of high-concentration or low-concentration are sufficiently diluted to be uniform solutions and the final tiny particles have almost the same w_t.

4 Conclusions

(1) Large-scale water tank experiments were designed and conducted to investigate the diffusion characteristics of the deep-sea mining sediment plumes in flowing water under different discharge rates Q and initial sediment solution concentrations c. Viscosity, resuspension and free settlement tests of sediment solution were carried out to reveal the settling mechanism of the sediment solution during the diffusion process.

(2) The morphological characteristics of the plume diffusion in the flowing water can be divided into four stages: jet-spreading stage, settlement−rebounding−resettlement stage, diffusion−transportation stage and dilution−resettlement stage. Higher Q leads to the plume with a smaller initial incident angle, larger diffusion range, poorer stability and more complicated morphology. Higher c results in the plume with larger settling velocity, faster formation of high-concentration accumulation zone, better stability and clearer diffusion boundary.

(3) The plume concentration evolution has

three stages: rapid rising stage, rapid dropping stage and slow dropping to be almost unchanged stage. Higher Q makes the plume concentration grow and drop faster in the first and second stages, respectively, and to be lower in the third stage. Higher c causes the plume concentration to reach a higher peak faster in the first stage, decrease more quickly in the second stage, and be higher in the third stage.

(4) The viscosity of sediment solution is exponentially increased with the increase of its initial concentration. The resuspension and the free settling velocities of sediment solution varying with time have three stages (fast increasing, fast decreasing and slowly decreasing until stability) and two stages (fast decreasing and slowly decreasing until stability), respectively. The high-concentration solution has smaller rising rate, smaller dropping rate and larger final resuspension settling velocity. It has almost the same final free settling velocity as the low-concentration solution.

(5) Although the large-scale water tank experiment has limitations in simulating the complex ocean environment due to its size, it can monitor the morphological and concentration evolution characteristics of the plumes in a short period of time, and provide data for the theoretical model and numerical simulation of the deep-sea mining plume diffusion.

CRediT authorship contribution statement

Ze-lin LIU: Methodology, Investigation, Software, Visualization, Writing − Original draft, Writing − Review & editing; **Xiang WU:** Resources, Validation, Writing − Review & editing; **Qiu-hua RAO:** Methodology, Conceptualization, Funding acquisition, Project administration, Supervision; **Wei YI**, **Shi-ping CHEN** and **Hao ZHENG:** Validation.

Declaration of competing interest

The authors declare that they have no known competing financial interests or personal relationships that could have appeared to influence the work reported in this paper.

Acknowledgments

This work was supported by the Major Project of Hunan Natural Science Foundation, China (No. 2021JC0010), and the National Natural Science Foundation of China (No. 51274251).

References

[1] LIU Shi-hang, YANG Jian-min, LYU Hai-ning, SUN Peng-fei, ZHANG Bei. Experimental and numerical investigation of the effect of deep-sea mining vehicles on the discharge plumes [J]. Physics of Fluids, 2024, 36(3): 033358.

[2] SHA Fei, XI Ming-shuai, CHEN Xu-guang, LIU Xue-lin, NIU Hong-ying, ZUO Yu-hang. A recent review on multi-physics coupling between deep-sea mining equipment and marine sediment [J]. Ocean Engineering, 2023, 276: 114229.

[3] LIU Ze-lin, RAO Qiu-hua, YI Wei, HUANG Wei. A modified drag coefficient model for calculating the terminal settling velocity and horizontal diffusion distance of irregular plume particles in deep-sea mining [J]. Environmental Science and Pollution Research International, 2024, 31(23): 33848−33866.

[4] XIE Jing, CUI Yi-an, LIU Jian-xin, GUO You-jun, ZHANG Li-juan, LUO Yi-jian, ZHANG Peng-fei. A review on theory, modeling, inversion, and application of self-potential in marine mineral exploration [J]. Transactions of Nonferrous Metals Society of China, 2023, 33(4): 1214−1232.

[5] WANG Zhen-xing, YU Yun-jun, YE Tian-tian, FEI Jiang-chi, SONG Xin-yu, PENG Jian-wei, ZHOU Yao-yu, WU Hong-hua. Distribution characteristics and environmental risk assessment following metal(loid)s pollution incidents at Southwest China mining site [J]. Transactions of Nonferrous Metals Society of China, 2022, 32(12): 4062−4075.

[6] XU Feng, RAO Qiu-hua, MA Wen-bo. Turning traction force of tracked mining vehicle based on rheological property of deep-sea sediment [J]. Transactions of Nonferrous Metals Society of China, 2018, 28(6): 1233−1240.

[7] JONES D O, KAISER S, SWEETMAN A K, SMITH C R, MENOT L, VINK A, TRUEBLOOD D, GREINERT J, BILLETT D S M, ARBIZU P M, RADZIEJEWSKA T, SINGH R, INGOLE B, STRATMANN T, SIMON-LLEDO E, DURDEN J M, CLARK M R. Biological responses to disturbance from simulated deep-sea polymetallic nodule mining [J]. PLoS One, 2017, 12(2): e0171750.

[8] YAMAZAKI T, KAJITANI Y. Deep-sea environment and impact experiment to it [C]//Proceedings of 9th ISOPE Conference. Brest, France, 1999: 374−381.

[9] SITLHOU L, CHAKRABORTY P. Comparing deep-sea polymetallic nodule mining technologies and evaluating their probable impacts on deep-sea pollution [J]. Marine Pollution Bulletin, 2024, 206: 116762.

[10] WEAVER P P E, AGUZZI J, BOSCHEN-ROSE R E, COLAÇO A, DE STIGTER H, GOLLNER S, HAECKEL M, HAUTON C, HELMONS R, JONES D O B, LILY H, MESTRE N C, MOHN C, THOMSEN L. Assessing plume impacts caused by polymetallic nodule mining vehicles [J]. Marine Policy, 2022, 139: 105011.

[11] HAN Wen-liang, WANG Guang-qian, WU Bao-sheng, LIU Shao-jun, ZOU Wei-sheng. Water hammer in coarse-grained solid−liquid flows in hydraulic hoisting for ocean mining [J]. Transactions of Nonferrous Metals Society of China, 2002, 12(3): 508−513.

[12] MINGOTTI N, WOODS A W. Stokes settling and particle-laden plumes: Implications for deep-sea mining and volcanic eruption plumes [J]. Philosophical Transactions of

the Royal Society A — Mathematical Physical and Engineering Sciences, 2020, 378(2179): 20190532.
[13] OUILLON R, MUÑOZ-ROYO C, ALFORD M H, PEACOCK T. Advection–diffusion settling of deep-sea mining sediment plumes. Part 2: Collector plumes [J]. Flow, 2022, 2: E23.
[14] LIU Shi-hang, YANG Jian-min, LU Hai-ning, SUN Peng-fei, ZHANG Bei. A numerical investigation of the dynamic interaction between the deep-sea mining vehicle and sediment plumes based on a small-scale analysis [J]. Journal of Marine Science and Engineering, 2023, 11(7): 1458.
[15] ZHANG Bei, LU Hai-ning, YANG Jian-min, SUN Peng-fei, DENG Li-wen. Numerical and experimental study on ore-collecting characteristics of deep-sea seafloor massive sulfide [J]. Ocean Engineering, 2024, 310: 118729.
[16] MA Wen-bin, SCHOTT D, RHEE C V. Numerical calculations of environmental impacts for deep sea mining activities [J]. Science of the Total Environment, 2019, 652: 996−1012.
[17] ALEYNIK D, INALL M E, DALE A, VINK A. Impact of remotely generated eddies on plume dispersion at abyssal mining sites in the Pacific [J]. Scientific Reports, 2017, 7(1): 16959.
[18] RZEZNIK A J, FLIERL G R, PEACOCK T. Model investigations of discharge plumes generated by deep-sea nodule mining operations [J]. Ocean Engineering, 2019, 172: 684−696.
[19] LIN Yuan, WENG Zi-xin, GUO Jin, LIN Xing-shuang, PHAN-THIEN N, ZHANG Jian. Simulation study on the sediment dispersion during deep-sea nodule harvesting [J]. Journal of Marine Science and Engineering, 2023, 11: 10.
[20] BAI Tian-bao, ZHAO Yong, ZHOU Yin-qing, HUANG Kun. Numerical simulation and analysis of initial plume discharge of deep-sea mining [J]. Ocean Engineering, 2024, 310: 118794.
[21] SPEARMAN J, TAYLOR J, CROSSOUARD N, COOPER A, TURNBULL M, MANNING A, LEE M, MURTON B. Measurement and modelling of deep sea sediment plumes and implications for deep sea mining [J]. Scientific Reports, 2020, 10(1): 5075.
[22] MUÑOZ-ROYO C, OUILLON R, EL MOUSADIK S, ALFORD M H, PEACOCK T. An in situ study of abyssal turbidity-current sediment plumes generated by a deep seabed polymetallic nodule mining preprototype collector vehicle [J]. Science Advances, 2022, 8(38): eabn1219.
[23] JANKOWSKI J A, MALCHEREK A, ZIELKE W. Numerical modeling of suspended sediment due to deep-sea mining [J]. Journal of Geophysical Research: Oceans, 1996, 101(C2): 3545−3560.
[24] MUÑOZ-ROYO C, PEACOCK T, ALFORD M H, SMITH J A, LE BOYER A, KULKARNI C S, LERMUSIAUX P F J, HALEY P J Jr, MIRABITO C, WANG D Y, ADAMS E E, OUILLON R, BREUGEM A, DECROP B, LANCKRIET T, SUPEKAR R B, RZEZNIK A J, GARTMAN A, JU S J. Extent of impact of deep-sea nodule mining midwater plumes is influenced by sediment loading, turbulence and thresholds [J]. Communications Earth & Environment, 2021, 2(1): 148.
[25] GILLARD B, PURKIANI K, CHATZIEVANGELOU D, VINK A, IVERSEN M H, THOMSEN L. Physical and hydrodynamic properties of deep sea mining-generated, abyssal sediment plumes in the Clarion Clipperton Fracture Zone (eastern-central Pacific) [J]. Elementa: Science of the Anthropocene, 2019, 7: 5.
[26] BAINES W D. Entrainment by a plume or jet at a density interface [J]. Journal of Fluid Mechanics, 1975, 68(2): 309−320.
[27] MOTT R W, WOODS A W. On the mixing of a confined stratified fluid by a turbulent buoyant plume [J]. Journal of Fluid Mechanics, 2009, 623: 149−165.

深海采矿沉积物羽流在大型动水水槽试验中的扩散特性

刘泽霖[1]，吴 翔[1]，饶秋华[1]，易 威[1]，陈时平[2]，郑 皓[2]

1. 中南大学 土木工程学院，长沙 410075；
2. 长沙矿冶研究院有限责任公司 深海矿产资源开发利用技术国家重点实验室，长沙 410012

摘 要：现有的沉积物羽流试验大多采用小规模的静水条件而很少采用大规模的动水条件进行。本文通过设计和开展大型动水水槽试验，研究深海采矿沉积物羽流在不同排放速率(Q)和初始浓度(c)下的扩散形貌和浓度演化特征；并通过开展不同浓度沉积物溶液的黏度试验、再悬浮试验和自由沉降试验，揭示羽流扩散过程中的沉降机理。结果表明：羽流在动水中扩散形貌特征变化分为 4 个阶段，羽流浓度变化呈现 3 个阶段。随着 Q 的增大，排放口羽流的初始入射角变小，扩散范围增大，稳定性降低和扩散模式更复杂。随着 c 的增大，羽状流的沉降速度增大，高浓度积聚区形成更快、稳定性更好和扩散边界更清晰。研究结果可为深海采矿对海洋环境影响的评价提供实验数据。

关键词：深海采矿；沉积物羽流；扩散特征；动水；大型水槽试验

(Edited by Wei-ping CHEN)